

# Resonant frequency and instability of multi-layered micro-resonators with initial imperfection subject to piezoelectric loads

Il-Kwon Oh <sup>\*</sup>, Dong-Weon Lee

*School of Mechanical Systems Engineering, Chonnam National University, 300 Yongbong-dong, Buk-gu, Gwang-Ju 500 757, Republic of Korea*

Available online 2 February 2007

## Abstract

The possibility to control the mistuned resonant frequency of multi-layered micro-resonators by piezoelectric actuations is numerically investigated. In many cases, there are mismatches of resonant frequency and initial imperfections of the multi-layered micro-resonators because of fabrication errors due to the difficulty of resolution control and mismatches of material properties. In this study, the multi-layered micro-resonators with initial imperfections were modeled by using refined layerwise theory and initial thermal loading. The nonlinear deformation and its attendant vibration characteristics of un-symmetrically deposited camped–camped micro-beams under piezoelectric and thermal actuations are extensively investigated. To derive the governing nonlinear finite element equations of the micro-beams, the incremental total Lagrangian description based on the multi-field layerwise theory is applied, considering geometric nonlinear strains and material inhomogeneity of multi-layered micro-resonators. Present results show that piezoelectric actuations can effectively tune the resonant frequencies of the imperfect multi-layered micro-resonators by controlling the in-plane and out-of-plane displacements.

© 2007 Elsevier B.V. All rights reserved.

*Keywords:* Resonator; Instability; Imperfection; Piezoelectric

## 1. Introduction

Because the multi-layered structures have several advantages resulting from integrated packaging and simple geometry, some researchers have attention to the multi-layered micro-resonators capable of tuning the resonant frequency. Micro-scale applications of thin-film micro-electro-mechanical structures for sensing and actuation require both integrated multi-layered structures and energy conversions between several physical fields. The multi-layered structures consist of silicon, silicon dioxide, silicon nitride, metallic electrodes, and piezoelectric layers. The thermal expansion mismatch between the constituting materials and the intrinsic stresses during deposition processing lead to undesired transverse deformations and residual stresses. There are mismatches of resonant frequency and initial imperfections of the multi-layered

micro-resonators because of fabrication errors due to the difficulty of resolution control and mismatch of material properties. Also, micro-machining errors and initial imperfection can change the resonant frequency and the quality factor of the structures. Therefore, the necessity to tune the resonant frequency of micro-resonators results from both fabrication errors and multi-purpose functionalities.

Lee and Cho [1] proposed a triangular electrostatic comb array for micro-mechanical resonant frequency tuning. A 3.3% reduction of the resonant frequency was observed from the initial resonant frequency of 2.42 kHz with the tuning voltage of 20 V. Syms [2] explored the electro-thermal actuator to tune the resonant frequency of folded and coupled vibrating micro-mechanical resonators. Remtema and Lin [3] tuned the active frequency of comb-shape micro-resonators by means of localized stressing effects originated from the Joule heating. Piazza et al. [4] investigated the voltage-tunable characteristics of piezoelectric multi-layered resonators.

<sup>\*</sup> Corresponding author. Tel.: +82 62 530 1685; fax: +82 62 530 1689.  
E-mail address: [ikoh@chonnam.ac.kr](mailto:ikoh@chonnam.ac.kr) (I.-K. Oh).

Some papers have addressed the flat multi-layered resonators using ZnO [5] and piezoelectric aluminum nitride [6]. Thermo-mechanical and electro-mechanical behaviors of multi-layered structures should be first dealt with on the design of micro-scale sensors and actuators. The deformation, stresses and vibration characteristics of multi-layered deformable elastic micro-structures are very complex under the applications of thermal loads and electric potentials due to buckling, postbuckling, snap-through and highly nonlinear behaviors. Chiao and Lin [7] analyzed electro-thermal and thermoelastic responses of micro-machined beams considering buckling behavior under resistive heating. Dunn et al. [8] studied the thermoelastic linear and nonlinear deformations of polysilicon/gold square and circular micro-plates subjected to uniform temperature changes. Xu et al. [9] presented a nonlinear finite element model of thin piezoelectric laminates and reported strong nonlinear relationship between the terminal voltage and deflections.

The multi-layered micro-resonators are relatively thick with respect to aspect ratio for high resonant frequency over MHz–GHz and has different constituent materials. Unlike homogeneous isotropic materials, multi-layered structures often result in the many unique phenomena including complex coupling between bending, extension and shearing modes, significant transverse shear deformation at lower thickness-to-span ratios and various damage from stress concentration near material and geometric discontinuities. In order to accurately analyze the very thick multi-layered micro-resonators, which is integrated with electro-thermal actuator and local piezoelectric layered sensors and actuators, more refined laminate theory that accounts for transverse shear effect and localized stresses and strains at the ply level, requiring layerwise model or 3D elasticity theory.

In this study, both thermal and piezoelectric actuators capable of in-plane and out-of-phase actuations will be studied for the implementation of the eccentrically multi-layered tunable resonators. The Hamilton's variational principle based on multi-field layerwise theory is applied for the nonlinear finite element modeling considering the geometric nonlinear effect on the stiffness variation. The effects of the piezoelectric eccentric actuation on changes of resonant frequency of multi-layered micro-resonators are extensively investigated.

## 2. Layerwise finite element modeling

In this study, the multi-field layerwise theory [10,11] including displacement, temperature and electric potential fields are proposed for the accurate description and the complex geometry of distributed and multi-layered piezoelectric sensors and actuators. In this approach the continuum displacements of the equilibrium equations are approximated through interpolation functions and the values of displacement at discrete points within the domain and on the boundary of the structures. By introducing

the piecewise interpolation function,  $\Phi^j(z)$ , along thickness direction and finite element shape functions  $\psi_j(\xi, \eta)$ , the multi-field layerwise descriptions are given as follows:

$$\begin{aligned} u_1 &= \sum_{i=1}^{\text{NID}} U^i(x, y, t) \Phi^i(z) = \sum_{i=1}^{\text{NID}} \sum_{j=1}^{\text{NPE}} U_j^i(x_j, y_j) \psi_j(\xi, \eta) \Phi^i(z), \\ u_2 &= \sum_{i=1}^{\text{NID}} V^i(x, y, t) \Phi^i(z) = \sum_{i=1}^{\text{NID}} \sum_{j=1}^{\text{NPE}} V_j^i(x_j, y_j) \psi_j(\xi, \eta) \Phi^i(z), \\ u_3 &= W(x, y, t) = \sum_{j=1}^{\text{NPE}} W_j^i(x_j, y_j) \psi_j(\xi, \eta), \\ \Delta T &= \sum_{i=1}^{\text{NID}} \Delta T^i(x, y, t) \Phi^i(z) = \sum_{i=1}^{\text{NID}} \sum_{j=1}^{\text{NPE}} \Delta T_j^i(x_j, y_j) \psi_j(\xi, \eta) \Phi^i(z), \\ E &= \sum_{i=1}^{\text{NID}} E^i(x, y, t) \Phi^i(z) = \sum_{i=1}^{\text{NID}} \sum_{j=1}^{\text{NPE}} E_j^i(x_j, y_j) \psi_j(\xi, \eta) \Phi^i(z). \end{aligned} \quad (1)$$

Here,  $u_1$ ,  $u_2$  and  $u_3$  are the elastic displacements in the  $x$ ,  $y$  and  $z$  direction, respectively.  $\Delta T$  and  $E$  are the temperature distribution and electric fields. The in-plane displacements, temperature distribution, electric fields can be described as a zigzag configuration by Lagrangian interpolation function along thickness direction. The NID means the number of sub-lamina of the plates with degree of freedoms.

The von-Karman nonlinear strain–displacement relationship is adopted to consider a transverse large deflection with small strains, which is the major factor of the nonlinear behavior of the multi-layered micro-structures with clamped or simply-supported boundary conditions each sides.

$$\begin{aligned} \varepsilon_{11} &= \frac{\partial u_1}{\partial x} + \frac{1}{2} \left( \frac{\partial u_3}{\partial x} \right)^2, & \varepsilon_{22} &= \frac{\partial u_2}{\partial y} + \frac{1}{2} \left( \frac{\partial u_3}{\partial y} \right)^2, & \varepsilon_{33} &= \frac{\partial u_3}{\partial z} \\ \varepsilon_{12} &= \frac{\partial u_1}{\partial y} + \frac{\partial u_2}{\partial x} + \frac{\partial u_3}{\partial x} \frac{\partial u_3}{\partial y}, & \varepsilon_{23} &= \frac{\partial u_3}{\partial y} + \frac{\partial u_2}{\partial z}, \\ \varepsilon_{13} &= \frac{\partial u_3}{\partial x} + \frac{\partial u_1}{\partial z}. \end{aligned} \quad (2)$$

The geometric nonlinearity is taken into account for large deflections, but the strain terms are assumed to be small so that the linear constitutive relationship is applied. The second Piola–Kirchhoff stress tensor is conjugated to the Green–Lagrangian strain tensor in that their properties are also invariant under rigid body motion. When the equilibrium of the body at time  $t + \Delta t$  is first expressed using Hamilton's principle of virtual displacements with tensor notation, the total Lagrangian formulation requires that

$$\begin{aligned} \int_V {}^{t+\Delta t} \mathbf{S}_{ij} \delta {}^{t+\Delta t} \varepsilon_{ij} \, dV &= {}^{t+\Delta t} W_u = \int_S {}^{t+\Delta t} T_k \delta u_k \, dS \\ &+ \int_V ({}^{t+\Delta t} f_k - \rho_k {}^{t+\Delta t} \ddot{u}_k) \delta u_k \, dV \end{aligned} \quad (3)$$

and

$$\int_V {}^{t+\Delta t}\mathbf{D}_k \delta^{t+\Delta t}\mathbf{E}_k dV = {}^{t+\Delta t}W_\phi = \int_{S_Q} {}^{t+\Delta t}Q \delta\phi dS, \quad (4)$$

where the  ${}^{t+\Delta t}\mathbf{S}_{ij}$ ,  ${}^{t+\Delta t}\boldsymbol{\varepsilon}_{ij}$ ,  ${}^{t+\Delta t}W_u$ ,  ${}^{t+\Delta t}T_k$ ,  ${}^{t+\Delta t}f_k$ ,  ${}^{t+\Delta t}\ddot{u}_k$ ,  $\rho_k$  and  $\delta u_k$  are the second Piola–Kirchhoff stress tensor, the total Green–Lagrangian strain tensor, the external virtual work, the surface traction components, the body force components, the current acceleration component, the density and the variation of the current displacement component defined at time  $t + \Delta t$ , respectively, referred to the initial configuration. Also,  ${}^{t+\Delta t}\mathbf{D}_k$ ,  ${}^{t+\Delta t}\mathbf{E}_k$ ,  ${}^{t+\Delta t}W_\phi$ ,  ${}^{t+\Delta t}Q$  and  $\delta\phi$  are the electric displacements, the electric field, the electric virtual work, the surface charge and the variation of electric potential.

The increments in several variables from the previous configuration at time  $t + \Delta t$  to current configuration at time  $t$  are defined as

$$\begin{aligned} {}^{t+\Delta t}\mathbf{S}_{ij} &= {}^t\mathbf{S}_{ij} + \mathbf{S}_{ij}, \\ {}^{t+\Delta t}\boldsymbol{\varepsilon}_{ij} &= {}^t\boldsymbol{\varepsilon}_{ij} + \boldsymbol{\varepsilon}_{ij}, \\ {}^{t+\Delta t}\mathbf{D}_k &= {}^t\mathbf{D}_k + \mathbf{D}_k, \\ {}^{t+\Delta t}\mathbf{E}_k &= {}^t\mathbf{E}_k + \mathbf{E}_k \end{aligned} \quad (5)$$

Here, the incremental strains  $\boldsymbol{\varepsilon}_{ij}$  comprise of the pure linear part, the linearized part and nonlinear terms as

$$\boldsymbol{\varepsilon}_{ij} = \mathbf{e}_{ij}^L + \mathbf{e}_{ij}^{LN} + \mathbf{e}_{ij}^N. \quad (6)$$

The linear constitutive equations of a thermopiezoelectric material with the assumption of the quasi-steady temperature distribution can be written. Noting that  $\delta^{t+\Delta t}\boldsymbol{\varepsilon}_{ij} = \delta\boldsymbol{\varepsilon}_{ij} = \delta\mathbf{e}_{ij}^L + \delta\mathbf{e}_{ij}^{LT} + \delta\mathbf{e}_{ij}^N$  and substituting Eqs. (5) and (6) into the left hand side of the Eq. (3) yield the following nonlinear equilibrium equations. Based on the virtual work of the elastic and electronic fields, the approximate nonlinear equilibrium equations are obtained as

$$\begin{aligned} &\int_V \rho_k {}^{t+\Delta t}\ddot{u}_k \delta u_k dV + \int_V \mathbf{C}_{ijkl} (\mathbf{e}_{kl}^L \delta\mathbf{e}_{ij}^L + \mathbf{e}_{kl}^L \delta\mathbf{e}_{ij}^{LT} + \mathbf{e}_{kl}^{LT} \delta\mathbf{e}_{ij}^L \\ &+ \mathbf{e}_{kl}^{LT} \delta\mathbf{e}_{ij}^{LT}) dV + \int_V \boldsymbol{\eta}_{km} ({}^t\widehat{\boldsymbol{\sigma}}_{mn} - {}^t\widehat{\boldsymbol{\tau}}_{mn} - {}^t\widehat{\boldsymbol{\zeta}}) \delta\boldsymbol{\eta}_{km} dV \\ &- \int_V e_{ijm} E_m (\delta\mathbf{e}_{ij}^L + \delta\mathbf{e}_{ij}^{LT}) dV \\ &= \int_S {}^{t+\Delta t}T_k \delta u_k dS + \int_V {}^{t+\Delta t}f_k \delta u_k dV - \int_V ({}^t\boldsymbol{\sigma}_{ij} - {}^t\boldsymbol{\tau}_{ij} - {}^t\boldsymbol{\zeta}_{ij}) \\ &\quad \times (\delta\mathbf{e}_{ij}^L + \delta\mathbf{e}_{ij}^{LT}) dV \end{aligned} \quad (7)$$

and

$$\begin{aligned} &\int_V (e_{kij} (\mathbf{e}_{ij}^L + \mathbf{e}_{ij}^{LT}) + \theta_{km} E_m) \delta E_k dV \\ &= \int_{S_Q} {}^{t+\Delta t}Q \delta\phi dS - \int_V {}^t\mathbf{D}_k \delta E_k dV. \end{aligned} \quad (8)$$

Consequently, we can drive the two coupled dynamic equations between mechanical and electric fields. The basic step in the derivation of the finite element equations is

based on the above virtual work functional in Eqs. (7) and (8). A general nonlinear displacement-based finite element formulation is presented with Lagrangian shape functions and the isoparametric description of the coordinates and displacements. Through the assembly process, the global governing equations can be expressed by the nodal displacement vector  $\mathbf{U}$  and the nodal electric potential  $\boldsymbol{\Phi}$  in the following form:

$$\begin{aligned} &\begin{bmatrix} \mathbf{M} & \mathbf{0} \\ \mathbf{0} & \mathbf{0} \end{bmatrix} \begin{bmatrix} \ddot{\mathbf{U}} \\ \ddot{\boldsymbol{\Phi}} \end{bmatrix} + \begin{bmatrix} \mathbf{K}^L - \mathbf{K}_{\Delta T}^G - \mathbf{K}_P^G + \mathbf{K}^N & \mathbf{K}_{U\Phi} \\ & \mathbf{K}_{\Phi\Phi} \end{bmatrix} \begin{bmatrix} \mathbf{U} \\ \boldsymbol{\Phi} \end{bmatrix} \\ &= \begin{bmatrix} \mathbf{F}_U^{\text{Ext}} - \mathbf{F}_U^{\text{Int}} \\ \mathbf{F}_\Phi^{\text{Ext}} - \mathbf{F}_\Phi^{\text{Int}} \end{bmatrix} \end{aligned} \quad (9)$$

Here  $\mathbf{M}$ ,  $\mathbf{K}^L$ ,  $\mathbf{K}_{\Delta T}^G$ ,  $\mathbf{K}_P^G$ ,  $\mathbf{K}^N$ ,  $\mathbf{K}_{U\Phi}$  and  $\mathbf{K}_{\Phi\Phi}$  mean the mass, linear stiffness, thermal geometric, piezoelectric geometric, nonlinear stiffness, piezoelectric-mechanical coupling and piezoelectric stiffness matrices, respectively. Especially, thermal and piezoelectric geometric matrices are originated from the modified geometric stresses  ${}^t\widehat{\boldsymbol{\tau}}_{mn}$  and  ${}^t\widehat{\boldsymbol{\zeta}}_{mn}$ . By the method of Guyan reduction, the above equations are simplified as

$$\begin{aligned} &\mathbf{M}\ddot{\mathbf{U}} + (\mathbf{K}^L - \mathbf{K}_{\Delta T}^G - \mathbf{K}_P^G + \mathbf{K}^N - \mathbf{K}_{U\Phi}\mathbf{K}_{\Phi\Phi}^{-1}\mathbf{K}_{\Phi U})\mathbf{U} \\ &= (\mathbf{F}_U^{\text{Ext}} - \mathbf{F}_U^{\text{Int}}) - \mathbf{K}_{U\Phi}\mathbf{K}_{\Phi\Phi}^{-1}(\mathbf{F}_\Phi^{\text{Ext}} - \mathbf{F}_\Phi^{\text{Int}}). \end{aligned} \quad (10)$$

Here, the small vibration under large deformations by piezoelectric and thermal actuations is assumed in the following form

$$\mathbf{U}(t) \cong \mathbf{U}_S + \mathbf{U}_D(t). \quad (11)$$

By substituting Eq. (11) into (10), we can obtain the unbalanced static and free vibration equations by the assumption of no dynamic excitations.

$$\begin{aligned} \mathbf{e}(\mathbf{U}_S) &= (\mathbf{K}^L - \mathbf{K}_{\Delta T}^G - \mathbf{K}_P^G + \mathbf{K}^N)(\mathbf{U}_S) - \mathbf{K}_{U\Phi}\mathbf{K}_{\Phi\Phi}^{-1}\mathbf{K}_{\Phi U}\mathbf{U}_S \\ &\quad - (\mathbf{F}_U^{\text{Ext}} - \mathbf{F}_U^{\text{Int}}(\mathbf{U}_S)) + \mathbf{K}_{U\Phi}\mathbf{K}_{\Phi\Phi}^{-1}(\mathbf{F}_\Phi^{\text{Ext}} - \mathbf{F}_\Phi^{\text{Int}}(\boldsymbol{\Phi}_S)) \end{aligned} \quad (12)$$

and

$$\mathbf{M}\ddot{\mathbf{U}}_D + \mathbf{K}^T(\mathbf{U}_S)\mathbf{U}_D = \mathbf{0}. \quad (13)$$

In order to solve the unbalanced static equations, next step is to linearize the above nonlinear error equations using iterative Newton–Raphson method.

$$\mathbf{e}_L(\mathbf{U}_S^{k+1}) = \mathbf{e}(\mathbf{U}_S^k) + \mathbf{K}^T(\mathbf{U}_S^k)(\mathbf{U}_S^{k+1} - \mathbf{U}_S^k) = \mathbf{0}, \quad (14)$$

where  $\mathbf{K}^T$  is the tangent stiffness matrix in the Eqs. (13) and (14). The resulting incremental equations can be expressed as

$$\mathbf{K}^T(\mathbf{U}_S^k)(\Delta\mathbf{U}^{k+1}) = -\mathbf{e}(\mathbf{U}_S^k), \quad (15)$$

where

$$\mathbf{K}^T(\mathbf{U}_S^k) = \mathbf{K}^L - \mathbf{K}_{\Delta T}^G - \mathbf{K}_P^G + \widehat{\mathbf{K}}^N(\mathbf{U}_S^k) - \mathbf{K}_{U\Phi}\mathbf{K}_{\Phi\Phi}^{-1}\mathbf{K}_{\Phi U} \quad (16)$$

$$\begin{aligned} \mathbf{e}(\mathbf{U}_S^k) &= (\mathbf{K}^L - \mathbf{K}_{\Delta T}^G - \mathbf{K}_P^G + \mathbf{K}^N)(\mathbf{U}_S^k) - \mathbf{K}_{U\Phi}\mathbf{K}_{\Phi\Phi}^{-1}\mathbf{K}_{\Phi U}\mathbf{U}_S^k \\ &\quad - (\mathbf{F}_U^{\text{Ext}} - \mathbf{F}_U^{\text{Int}}(\mathbf{U}_S^k)) + \mathbf{K}_{U\Phi}\mathbf{K}_{\Phi\Phi}^{-1}(\mathbf{F}_\Phi^{\text{Ext}} - \mathbf{F}_\Phi^{\text{Int}}(\boldsymbol{\Phi}_S^k)). \end{aligned} \quad (17)$$

Also, updated iterative displacement are related to incremental displacements as

$$\mathbf{U}_S^{k+1} = \mathbf{U}_S^k + \Delta \mathbf{U}^{k+1} \tag{18}$$

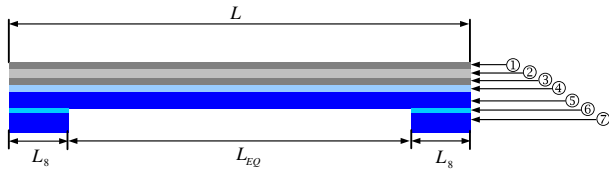
After obtaining the converged nonlinear static solutions,  $\mathbf{U}_S$ , the free vibration analysis can be performed by solving the Eq. (13) as an eigenvalue problem under the assumption of small harmonic oscillation.

$$(\mathbf{K}^T(\mathbf{U}_S) - \omega^2 \mathbf{M}) \tilde{\mathbf{U}}_D = \mathbf{0} \tag{19}$$

Here,  $\omega$  is the natural frequency and  $\tilde{\mathbf{U}}_D$  is the natural mode vector.

### 3. Results and discussion

In this study, the eccentrically multi-layered micro-resonators are analyzed for the design of tunable resonators as shown in Fig. 1 and described in Table 1. All multi-layered resonators have un-symmetric lay-up through thickness direction. The wafer used in this study has a full length driving electrode without a sensing electrode. Actually, this wafer can be implemented with sensing and driving functions by using the concept of the sensory actuators. Here, the equivalent length  $L_{EQ}$  means un-clamped length of the bottom surface. The equivalent lengths of  $L_{EQ} = 400 \mu\text{m}$ , and a typical total thickness of  $h_{EQ} = 3.3 \mu\text{m}$  are used in



① Driving electrode (Pt), ② PZT active layer, ③ Grounded electrode (Ti, Pt),  
④ Electric insulation layer (Silicon Nitride), ⑤ Silicon,  
⑥ Silicon dioxide, ⑦ Anchor (Silicon)

Fig. 1. Geometry and constituents of multi-layered micro-resonators.

Table 1  
Geometry of un-symmetric multi-layered micro-resonator (Unit:  $\mu\text{m}$ )

Wafer	$L_{EQ}$	$L$	$L_8$	$W$	$h_1, h_2, h_4$	$h_3$	$h_5$	$h_6$	$h_7$	$h_8$
1	400	480	40	20	0.15	0.5	0.5	2	1	4

Table 2  
Material properties of substrate layers

Properties	Silicon nitride ( $\text{Si}_3\text{N}_4$ )	Silicon dioxide ( $\text{SiO}_2$ )	Silicon (Si)	Electrodes (Pt)	PZT layer
Young's modulus (GPa)	300	70	165	147	63
Poisson's ratio ( $\nu$ )	0.27	0.17	0.22	0.39	0.3
Density ( $\text{kg/m}^3$ )	3180	2200	2330	2150	7600
Thermal expansion coefficient ( $\alpha, 10^{-6}/\text{K}$ )	3.3	0.5	2.6	8.9	0.9
Thermal conductivity ( $\text{W/mK}$ )	20	1.1	67.5	69.23	27.2
Piezoelectric charge coefficient (pm/V)	0	0	0	0	$d_{31} = 254$ $d_{32} = 254$
Dielectric permittivity (nf/m)	0	0	0	0	15.3

the following analyses and figures. The substrate multi-layers consist of silicon, silicon nitride, silicon dioxide, platinum electrodes and PZT, and the material properties are written in Table 2. In order to design a tunable multi-layered resonator, both piezoelectric and thermal actuations are numerically simulated with a special concern about the change of the resonant frequency as well as transverse center deflections.

The initial imperfection is taken into account by using thermal deformation. The four different thermal loading conditions of  $\Delta T/\Delta T_{CR} = 0.1, 1.0, 2.0, 3.0$  are used. Here,  $\Delta T_{CR} = 16.33^\circ\text{C}$  means Euler buckling temperature. As the thermal load increases, the initial thermal deflection increases. Fig. 2 shows the nonlinear static deflections at the center point as the piezoelectric potential decreases with

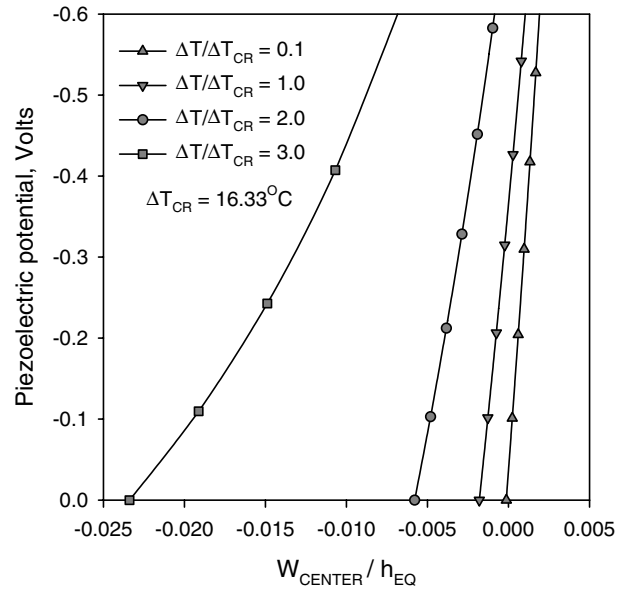


Fig. 2. Nonlinear static deflections of multi-layered micro-resonators with thermally initial imperfection under compressive piezoelectric actuation.

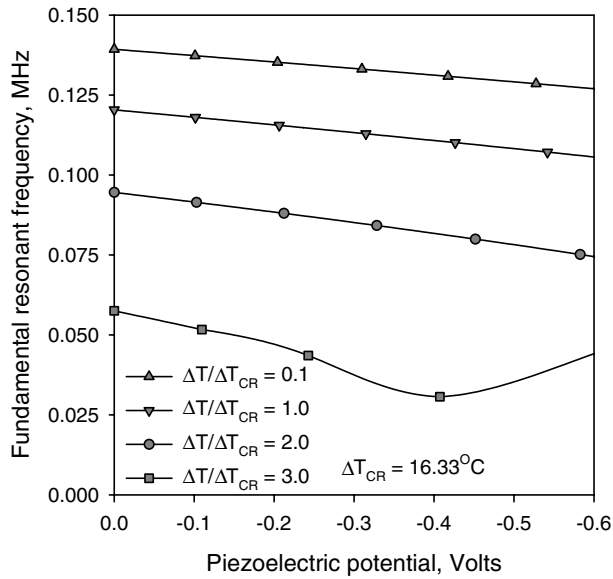


Fig. 3. Fundamental resonant frequency of multi-layered micro-resonators with thermally initial imperfection under compressive piezoelectric actuation.

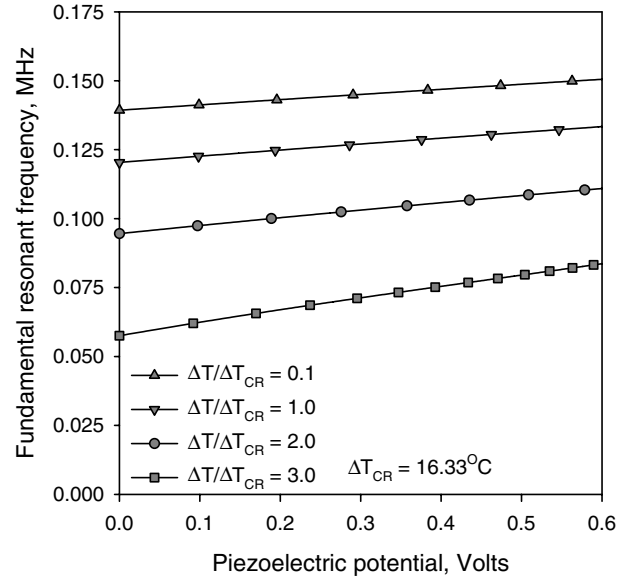


Fig. 5. Fundamental resonant frequency of multi-layered micro-resonators with thermally initial imperfection under tensile piezoelectric actuation.

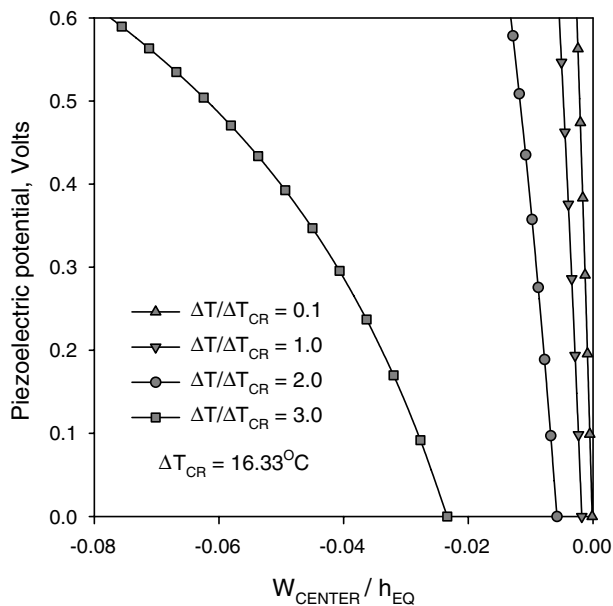


Fig. 4. Nonlinear static deflections of multi-layered micro-resonators with thermally initial imperfection under tensile piezoelectric actuation.

negative values. The nonlinear center deflection decreases to zero and shows positive values in some cases with decreasing piezoelectric potential. Its attendant vibration characteristics are shown in Fig. 3. The fundamental resonant frequency decreases as the piezoelectric potential decreases with negative values. Fig. 4 shows the nonlinear static deflections at the center point as the piezoelectric potential increases with positive values. The nonlinear cen-

ter deflection increases with negative values with increasing piezoelectric potential. The change of fundamental resonant frequency is shown in Fig. 5. The fundamental resonant frequency increases as the piezoelectric potential increases with positive values. Present results show that we can easily control and tune the mistuned resonant frequency of multi-layered micro-resonators with initial imperfections by using piezoelectric actuation.

#### Acknowledgement

This work was supported by the Korea Research Foundation Grant (KRF-2004-003-D00016), in which main calculations were performed by using the supercomputing resources of the Korea Institute of Science and Technology Information (KISTI).

#### References

- [1] K.B. Lee, Y.H. Cho, *Sensors and Actuators A* 70 (1998) 112.
- [2] R.R.A. Syms, *J. Microelectromechanical Syst.* 7 (1998) 164.
- [3] T. Remtema, L. Lin, *Sensors and Actuators A* 91 (2001) 326.
- [4] G. Piazza, R. Abdolvand, G.K. Ho, F. Ayazi, *Sensors and Actuators A* 111 (7) (2004) 71.
- [5] D.L. DeVoe, *Sensors and Actuators A* 88 (2001) 263.
- [6] E. Iborra, J. Olivares, M. Clement, L. Vergara, A. Sanz-Hervas, J. Sangrador, *Sensors and Actuators A* 115 (2004) 501.
- [7] M. Chiao, L. Lin, *J. Microelectromechanical Syst.* 9 (2000) 146.
- [8] M.L. Dunn, Y. Zhang, V.M. Bright, *J. Microelectromechanical Syst.* 11 (2002) 372.
- [9] C.G. Xu, T.S. Fiez, K. Mayaram, *J. Microelectromechanical Syst.* 12 (2003) 649.
- [10] I.K. Oh, J.H. Han, I. Lee, *J. Sound Vib.* 233 (2000) 19.
- [11] I.K. Oh, J.H. Han, I. Lee, *AIAA J.* 39 (2001) 1188.